JACS
JOURNAL OF THE AMERICAN CHEMICAL SOCIETY
Article
pubs.acs.org/JACS

First-Principles Study of the Role of O_2 and H_2O in the Decoupling of Graphene on Cu(111)

Kester Wong,[†,‡] Seok Ju Kang,[‡] Christopher W. Bielawski,[†,‡,§] Rodney S. Ruoff,*[,†,§,∥] and Sang Kyu Kwak*[,†,‡]

[†]Center for Multidimensional Carbon Materials (CMCM), Institute for Basic Science (IBS), Ulsan 44919, Republic of Korea
[‡]School of Energy and Chemical Engineering, [§]Department of Chemistry, School of Natural Sciences, and [∥]School of Materials Science and Engineering, Ulsan National Institute of Science and Technology (UNIST), Ulsan 44919, Republic of Korea

Supporting Information

ABSTRACT: The structural and electronic properties of graphene coated on a Cu(111) surface can be strongly influenced by the arrangement of adsorbates at the graphene edges. Oxygen and water intercalation at the graphene edges could lead to oxidation and hydrolysis at the graphene/Cu(111) interface, eventually causing decoupling of graphene from the Cu substrate. However, the reaction pathways for oxygen or water (or both) intercalation at the graphene edges are not well understood at the molecular level. Using ab initio density functional theory calculations, we observed a strong hybridization of π orbitals at a zigzag edge of a graphene nanoribbon (GNR) on a bare Cu(111) surface, whereas such hybridization was absent for the corresponding armchair edge under otherwise identical conditions. These results indicate that the edge type influences the oxidation chemistry beneath the GNR. Moreover, we demonstrate that the presence of oxygen species, as well as GNR, facilitates the propagation of H_2O. The following decoupling mechanisms are discussed: (i) GNRs with armchair edge configurations on Cu(111) can be decoupled via a sequential reaction that involves O_2 dissociation followed by H_2O intercalation, whereas (ii) GNRs with zigzag edge configurations on Cu(111) can be decoupled by oxygen intercalation.

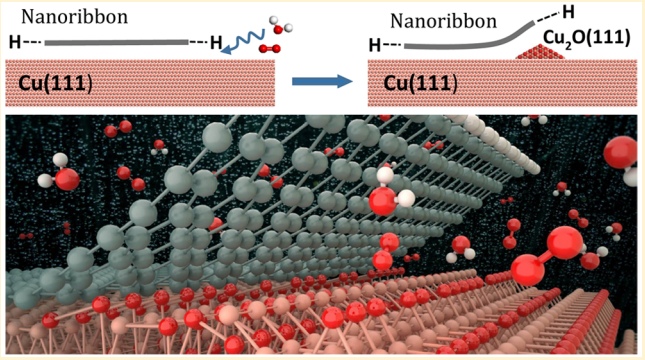

INTRODUCTION

Graphene is commonly grown on Cu substrates using chemical vapor deposition (CVD) methods largely due to the low solubility of C in Cu, which facilitates the formation of monolayers.[1] While conventional postgrowth graphene transfer processes tend to generate a considerable amount of defects in the material, recent developments have demonstrated that such costly and time-consuming procedures can be improved to obtain graphene with higher purities and lower concentrations of defects. Some of these methods include decoupling[2] and/or mechanical delamination[3] of CVD-grown graphene and are concomitant with the oxidation of the underlying Cu substrate. In some procedures, the Cu substrate may be recovered and reused.[3] While it has been demonstrated that graphene effectively "protects" the underlying copper from oxidation, oxidation can still occur, even on single-crystal Cu substrates covered with high-quality graphene.[4] Indeed, the carbon−metal interaction may accelerate electrochemical oxidation of the Cu substrate via galvanic corrosion,[5] as graphene is cathodic to Cu.[6,7]

These reactions are expected to proceed at different rates depending on the quality of the graphene coating and the Cu surface morphology. Atomic and molecular intercalations at various graphene/metal interfaces have been reported.[8−14] Previous experimental studies have indicated that O_2 intercalates the graphene-coated Cu substrate complex and contributes to the substrate oxidation as well as to graphene decoupling.[15] The reported oxidation was described as "fast", such that the intercalation−decoupling of graphene occurred within minutes to hours at room temperature. However, the rapid oxidation can be attributed to the polycrystalline Cu, which can have other low index surfaces with relatively high oxidation degree, such as the (100) and (124) facets.[16] Additionally, various spectroscopic techniques, including Raman,[2,17] X-ray photoelectron spectroscopy (XPS),[17] and normal incidence X-ray standing wave,[18] indicated that oxygen can penetrate through the grain boundaries in graphene and form a thin layer of cuprous oxide (Cu_2O) at the graphene/Cu interface. The presence of water has also been reported to promote oxidation and facilitate the decoupling of graphene grown via CVD from Cu substrates.[2,3,15] To the best of our knowledge, there has been no fundamental investigation of the mechanisms of these reactions, and it has not been clarified whether the oxidation originates from H_2O or O_2 (or both) adsorbed at the graphene/Cu(111) interface. Here, we explore

Received: May 24, 2016
Published: August 4, 2016

DOI: 10.1021/jacs.6b05333
J. Am. Chem. Soc. 2016, 138, 10986−10994

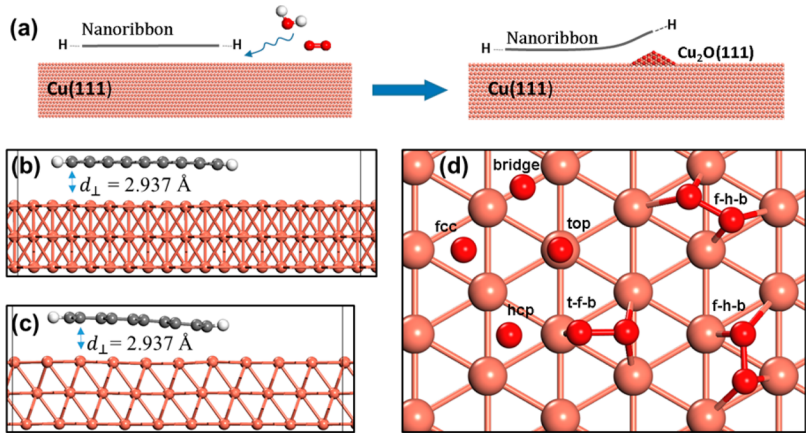

Figure 1. (a) Schematic of galvanic corrosion and the intercalation of O_2 and H_2O at the GNR-coated Cu interface via nanoribbon edges. The GNR, when in contact with the Cu surface, functions as a cathode, whereas the Cu functions as an anode. The direction of intercalation is indicated by the squiggly arrow. The oxide $Cu_2O(111)$ is represented by a cluster that protrudes from the Cu surface, which can be formed via chemical reactions with surrounding molecules. Side view of armchair (b) and zigzag (c) GNR on a Cu(111) surface; (d) top view of the top layer Cu atoms (pink) showing possible atomic and molecular adsorptions of O_2 (red) that can take place on the Cu(111) surface. The edges are H-terminated (white), with left-edged C atoms (gray) of the GNR fixed at a height of 2.937 Å; $d_\perp$. The notations *t*, *f*, *h*, and *b* denote the top, fcc, hcp, and bridge adsorption sites.

the chemical transformations of O_2 and H_2O on graphene-coated Cu substrates. Among the many reactions involving O_2 and H_2O molecules that can take place at the Cu(111) surface,[19,20] we considered two types of reactions: the dissociation of O_2 on Cu(111) (eq 1) and the dissociation of H_2O at the oxygen-doped Cu(111) surface (eq 2):

$$O_2 \rightarrow O_{ads} + O_{ads} \quad (1)$$

$$H_2O + O_{ads} \rightarrow OH_{ads} + OH_{ads} \quad (2)$$

These two reactions were selected due to the high sensitivity of graphene toward such oxygen-containing species.[21,22] Furthermore, the adsorption interaction energies of O (5.30 eV) and OH (3.26 eV) on Cu(111) are significantly higher than those of other small radicals or molecules,[20] which effectively renders these reactions more favorable.

Recent advances in CVD methods have enabled the growth of monocrystalline graphene on a Cu(111) surface.[23−26] The singly oriented graphene islands are confined by either zigzag-only or armchair-only edges. As a model for these edges in our calculations, we utilized graphene nanoribbons (GNR) containing armchair (aGNR)[27] or zigzag (zGNR)[28] edges terminated with hydrogen. Under room temperature and atmospheric pressure (the partial H_2 pressure in air is ~3.75 × 10^{-4} Torr[27]), it is most likely that the graphene edges are hydrogen-terminated and that the H_2 pressure (mTorr) is not low enough to indicate metal passivated edges.[29] Details on the construction of the GNR/Cu(111) models in unit cell are described in the Structural Models section. We first investigated single-molecule (O_2 and H_2O) adsorption at the aGNR/Cu(111) and zGNR/Cu(111) edge sites and identified O_2 and H_2O dissociation pathways at these interfaces. The intercalation of O_2 and H_2O at various GNR edge sites was also investigated, and it was found that the presence of oxygen-containing species, as well as GNR, significantly influences the dissociation of H_2O. A schematic representation of a GNR on a Cu(111) surface showing the oxidation processes initiating at the edge sites, followed by subsequent decoupling, is illustrated in Figure 1a.

COMPUTATIONAL DETAILS

Spin-polarized density functional theory (DFT) calculations were performed using the Vienna ab initio Simulation Package[30,31] within the projector-augmented wave scheme.[32] The generalized gradient approximation using the Perdew−Burke−Ernzerhof (PBE) functional was employed for the exchange-correlation potential.[33] Semiempirical corrections accounting for van der Waals (vdW) interactions were described by Grimme's D2 method.[34] A preliminary set of calculations employing the PBE and PBE-D2 functionals revealed that vdW corrections are essential to describe the GNR adsorption interaction on Cu(111) surfaces. When the PBE method was used for geometry optimization calculations, we observed that aGNR desorbed from the substrate into the vacuum space and the adsorption energy for zGNR/Cu was reduced. In contrast, we were able to obtain stable geometries for aGNR as well as zGNR on Cu using the PBE-D2 method. Therefore, all the results presented here have been calculated using the D2 method. A cutoff energy of 400 eV for the plane wave basis set was employed for all calculations with different *k*-point mesh sizes used for the Brillouin zone integration: 5 × 3 × 1 for aGNR/Cu(111) and 3 × 5 × 1 for zGNR/Cu(111). For the atomic position optimization, the stopping criteria before convergence was 10^{-5} eV for the electronic self-consistency loop, and the Hellmann−Feynman (ionic) forces converged to less than 0.013 eV/Å. The climbing image nudged elastic band (NEB) method[35,36] was employed for the determination of transition states and activation barriers using an electronic self-consistency loop stopping criteria of 1 × 10^{-5} eV, and the ionic forces converged to 0.020 eV/Å.

STRUCTURAL MODELS

While the graphene decoupling process may originate from edge-site molecular interactions, other factors such as defect, grain boundary, or solvation effects are not considered in this study. Efforts were focused on the adsorption of gas-phase molecules at various GNR/substrate interfaces. The aGNR and zGNR widths can be described by the parameters N_a for the number of zigzag lines and N_z for the number of dimer lines, respectively.[37] In our structural models, we have restricted the GNR width to four consecutive benzene-like rings. GNRs with similar widths have been previously employed to describe the oxygen intercalation mechanism of graphene on transition metals.[38] We note that the growth symmetry of graphene is dependent on the metal substrate and can adopt face-centered

DOI: 10.1021/jacs.6b05333
J. Am. Chem. Soc. 2016, 138, 10986−10994

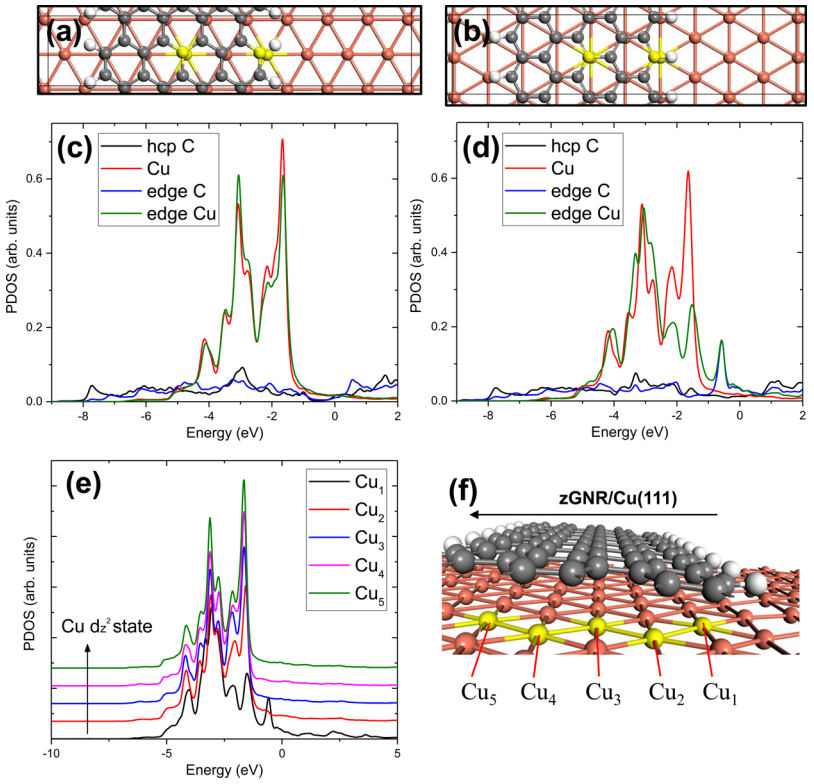

Figure 2. (a,b) Top view of armchair (left) and zigzag (right) graphene nanoribbons on the Cu(111) surface, showing only the top layer Cu atoms as viewed from above. Each unit cell (black line) corresponds to two C−H functional groups on each side of the nanoribbon edges. The selected C and Cu atoms are highlighted in yellow, in which their PDOS reflect the C $2p_z$ and Cu $3d_{z^2}$ orbitals for aGNR/Cu (c) and zGNR/Cu (d) interfaces. (e) PDOS of the Cu $3d_{z^2}$ orbitals for several Cu interface atoms in zGNR/Cu (f). The selected Cu atoms are highlighted in yellow, starting from a Cu atom directly below the zGNR edge C atom and moving toward another Cu atom, as indicated by the arrow.

cubic (fcc), hexagonal close-packed (hcp), and/or fcc−hcp graphene/metal arrangements.[39,40] Hence, we have constructed GNR/Cu(111) models with a hcp configuration that shares the same adsorbate−substrate reactivity as the fcc arrangement.[41] In the hcp configuration, a sublattice of C atoms was positioned above the topmost Cu atoms, while another set of C atoms was positioned at the hcp sites of the Cu lattice. We have used periodically repeating supercells consisting of a three-layered Cu(111) slab with the GNR positioned over one side of the slab (Figure 1b−d). A vacuum space of ∼10 Å was introduced in the direction perpendicular to the surface plane. A bulk lattice constant value of 2.555 Å for the Cu(111) substrate was considered for the graphene/Cu system as the graphene is stretched by ∼4% on Cu(111) surfaces.[42,43] Adsorbate(s) and the top two Cu layers were allowed to relax during the geometry optimization. The C−Cu interface separation distance for monolayer graphene on a Cu(111) surface was optimized to be 2.937 Å, in which the C atoms were sp^2-hybridized and thus unable to form chemical bonds with the Cu atoms.[44] To maintain any vdW interactions formed between the GNR and underlying Cu(111) substrate, the edge C atoms on one side of the GNR were fixed to a height of 2.937 Å, while allowing the other side of the GNR to relax on the surface. In this manner, the GNR decoupling processes can be simulated as other contributing factors such as sliding and lifting of the GNR are minimized.

■ ENERGY CALCULATIONS

We define the binding energy (BE) of the GNR adsorbed on a bare Cu(111) surface as well as on the intercalated system as follows (eqs 3.1 and 3.2, respectively):

$$\mathrm{BE_{GNR}} = \frac{E_{\mathrm{GNR/Cu(111)}} - (E_{\mathrm{Cu(111)}} + E_{\mathrm{GNR}})}{n} \quad (3.1)$$

and

$$\mathrm{BE_{GNR}} = \frac{E_{\mathrm{ads/GNR/Cu(111)}} - (E_{\mathrm{ads/Cu(111)}} + E_{\mathrm{GNR}})}{n} \quad (3.2)$$

where $E_{\mathrm{GNR/Cu(111)}}$ is the total energy of aGNR or zGNR adsorbed on the Cu(111) surface, $E_{\mathrm{Cu(111)}}$ is the energy of Cu(111), E_{GNR} is the energy of the GNR in a vacuum, n is the number of carbon atoms, and $E_{\mathrm{ads/GNR/Cu(111)}}$ and $E_{\mathrm{ads/Cu(111)}}$ are the total energies of the adsorbate molecule(s) on the Cu surface with and without GNRs, resepectively. In the latter energy term, it should be noted that we assume an artificial adsorption configuration for which all other atom positions remain unchanged when the GNR is removed.

Next, we calculate the adsorption energy and the dissociation barrier for O_2 at the aGNR and zGNR edge sites. The O_2 dissociation at the aGNR/Cu(111) and zGNR/Cu(111) interfaces is compared to that at the bare Cu(111) surface. The activation barrier of a chemical reaction, $E_a = E_{TS} - E_{IS}$, is defined by the energy difference between the reactant state (E_{IS}) and transition state (E_{TS}), while the reaction energy is given by $\Delta E = E_{IS} - E_P$, where E_P is the energy of the product. Negative and positive ΔE values are indicative of exothermic

DOI: 10.1021/jacs.6b05333
J. Am. Chem. Soc. 2016, 138, 10986−10994

and endothermic reactions, respectively. Additional geometry optimization calculations were performed with H_2O molecules inserted at the edges. Various reaction mechanisms for H_2O adsorption and intercalation at both GNR edges were identified. The adsorption energies for O_2 or H_2O adsorbed on a GNR/Cu(111) interface may be written as follows (eqs 4.1 and 4.2, respectively):

$$BE_{O_2} = E_{O_2/GNR/Cu(111)} - (E_{GNR/Cu(111)} + E_{O_2}) \quad (4.1)$$

and

$$BE_W = E_{H_2O/GNR/Cu(111)} - (E_{GNR/Cu(111)} + E_{H_2O}) \quad (4.2)$$

where $E_{O_2/GNR/Cu(111)}$ and $E_{H_2O/GNR/Cu(111)}$ are the total energies of all components in the respective systems and E_{O_2} and E_{H_2O} are the total energies of the free molecules of O_2 and H_2O in gas phase. Likewise, the coadsorption energy for the adsorbates may be calculated as follows (eq 5):

$$BE_{ads} = E_{ads/GNR/Cu(111)} - (E_{GNR/Cu(111)} + E_{H_2O} + E_{O_2}) \quad (5)$$

where $E_{ads/GNR/Cu(111)}$ is the total energy of adsorption for both O_2 and H_2O adsorbed at the GNR/Cu(111) interface. Negative binding energy values from eqs 3−5 are consistent with a thermodynamically favored adsorption interaction between the different oxygen-containing species and Cu(111).

RESULTS AND DISCUSSION

Below, we demonstrate that the GNR adsorption interaction on the surface of the Cu support is influenced by the O_2 and H_2O molecules at the GNR edges. The binding energies of the adsorbates (O_2, H_2O, aGNR, and/or zGNR) on the Cu surface as well as the distances between the nanoribbon edges and the surface, $d_\perp$(G-Cu_{sub}), are given in Tables S1 and S2 (see Supporting Information (SI)).

H-Terminated aGNR and zGNR on Cu(111). For the H-terminated aGNR and zGNR nanoribbons deposited on bare Cu(111) at the hcp site, the geometrically optimized structure and the electronic properties of the nanoribbon edge C atoms can be gleaned from Figure 1b−d. The binding energies calculated for the geometrically optimized aGNR/Cu(111) and zGNR/Cu(111) systems show that zGNR adsorbs more strongly (∼−0.13 eV per carbon atom) on the bare Cu(111) surface. The calculated C−Cu perpendicular distance ($d_\perp$) for zGNR/Cu(111) is also shorter (2.26 Å) than that calculated for aGNR/Cu(111) (2.77 Å). These results are consistent with previous studies of the adsorption of H-terminated zGNR on Cu(111), where a $d_\perp$ value of 2.37 Å at the edge site was reported.[45] Another difference, as yet unexplained, between the aGNR/Cu(111) and zGNR/Cu(111) systems is the presence of an edge state in the projected density of states (PDOS) of zGNR/Cu(111). The new peaks near the Fermi level that appeared in Figure 2d were attributed to hybridization of the $2p_z$ orbitals of the C atoms and the $3d_{z^2}$ orbitals of Cu atoms[46] and may indicate that the zGNR edges adopt a radical characteristic, at least partially.[47] However, the strong hybridization of the out-of-plane graphene π orbitals with the metal d bands is only observed for the edge C atoms and the Cu atoms directly beneath it; the edge state disappears for the neighboring Cu atoms (see Figure 2e,f). Such edge states are usually observed in metal-passivated zGNRs[45] and have not been reported for H-terminated zGNR/Cu(111) systems to the best of our knowledge. Further descriptions of the PDOS calculations are given in Figure S4. The small interface separation observed for the zGNR/Cu(111) interface can be described by a predominantly covalent interaction between the Cu and C atoms since the covalent bond length for Cu−C ranges from 2.04 to 2.17 Å.[48] Therefore, we conjecture that the aGNR shows a weaker adsorption interaction compared to that of the zGNR on Cu(111) surfaces given that both GNRs are adsorbed in the hcp configuration.

O_2 Adsorption Mechanism at the aGNR/Cu(111) and zGNR/Cu(111) Edges. The dissociative adsorption of O_2 at the aGNR/Cu(111) and zGNR/Cu(111) edge sites is shown with and without GNR in Figure 3a,b, respectively. The

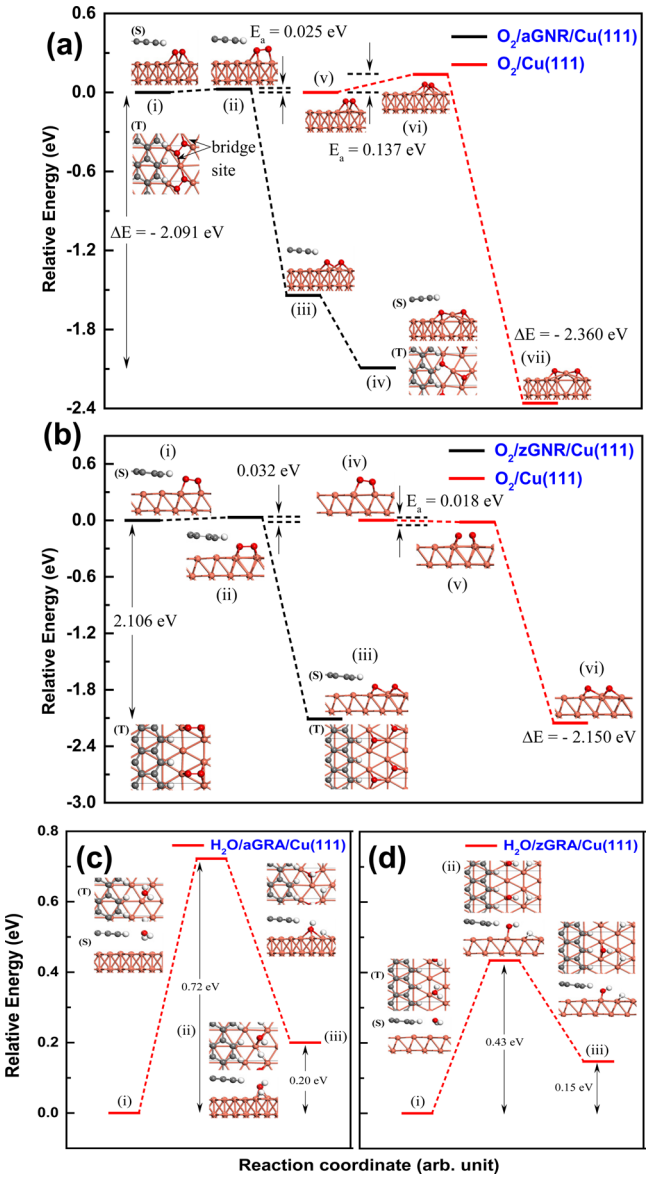

Figure 3. Climbing image nudged elastic band calculations showing top (T) and side (S) views. Dissociative adsorption of (a) O_2 at the aGNR/Cu interface (black) and at the bare Cu surface (red). Dissociative adsorption of (b) O_2 (black) at the zGNR/Cu interface and at the bare Cu surface (red). O_2 adapts the f-h-b and t-f-b adsorption configurations with or without the GNR at Cu (see Figure 1d for more details). Dissociative adsorption of H_2O at the (c) aGNR/Cu and (d) zGNR/Cu interfaces. The calculated activation barrier (E_a) and the energy difference (ΔE) are shown.

DOI: 10.1021/jacs.6b05333
J. Am. Chem. Soc. 2016, 138, 10986−10994

calculated BE values are presented in Tables S1 and S2. At the bare Cu(111) surface, we find that the O_2 molecule can adsorb at the f-h-b (Figure 3a) and t-f-b (Figure 3b) sites depicted in Figure 1d. The resulting NEB calculations show that the O_2 molecule dissociates at the Cu surface with a large energy drop (ΔE) of 2.15−2.36 eV, indicating that the chemisorption-induced displacement of the Cu atom is favored. The large ΔE values are in accordance with another study of O_2 dissociation at Cu(111) reported recently (ΔE = 2.11 eV).[38] The activation barrier (0.137 eV) for the dissociation of O_2 in the f-h-b configuration (Figure 3a(v)) is comparable to the value (0.103 eV) calculated by López-Moreno and Romero.[49] Additionally, Ford et al.[19] reported an activation barrier of 0.23 eV for the O_2 dissociation on Cu(111), using $p(2 \times 2)$ surface unit cells with four metal layers. The larger activation barrier can be attributed to the difference in the surface coverage, 1/4 monolayer (ML) per molecule, and the number of surface atomic layers considered in their study. However, our results are similar to experimentally determined activation energies for O_2 dissociation on Cu(111) using Auger electron spectroscopy (AES), low-energy electron diffraction, and ellipsometry (0.07−0.17 eV).[50] Outside of the GNR edge, O_2 readily dissociates into radical pairs and chemisorbs onto the Cu surface with almost negligible activation barriers at the aGNR and zGNR edge sites. The O_2 adsorbed more strongly at the aGNR/Cu and zGNR/Cu interfaces than on the bare Cu surface, indicating that the GNR stabilizes the adsorbate in its vicinity. For the aGNR/Cu(111) system (see Table S1 and Figure 3a(i)) on the bare Cu surface, O_2 adsorbs molecularly at the f-h-b site with a BE_{O_2} value of −0.87 eV. A similar adsorption configuration with a BE_{O_2} value of −0.75 eV has been previously reported.[49] When dissociated, the O radical pair adsorbs strongly on the surface with a BE value of −3.23 eV/pair (−1.62 eV/atom) in a bridge-type configuration between the fcc and hcp three-fold hollow sites. The activation barriers for the dissociative chemisorption of O_2 at aGNR/Cu (0.025 eV) as well as zGNR/Cu (0.032 eV) are smaller than the experimentally measured O diffusion barrier (0.25 eV)[51] and the theoretically calculated value of 0.26 eV/O_2 at 1/4 ML coverage on Cu(111).[52] The larger diffusion barrier offers some degree of "protection" for the metallic substrate from undergoing oxidation. For the zGNR/Cu(111) system, O_2 adsorbs molecularly on the bare Cu surface at the t-f-b site (see Table S2 and Figure 3b(i)) with a BE_{O_2} of −0.96 eV. A similar adsorption configuration with a BE_{O_2} value of −0.77 eV has been reported.[49] When dissociated, the O radical pair adsorb on the surface with a binding energy BE_{O_2} of −3.13 eV/pair (−1.57 eV/atom) with the O atoms positioned at three-fold hollow sites. We note that, even without the GNR, dissociative chemisorption of O_2 on Cu(111) is feasible, and the influence of the nanoribbon edges serves mainly to reduce the activation barrier for O_2 dissociation. The activation barrier for the graphene−Cu decoupling can be overcome by the energy gain from the dissociative/molecular adsorptions at the interface. As shown in Figure 3a,b, the dissociation of O_2 is exothermic at the aGNR/Cu as well as the zGNR/Cu interfaces, which means that the adsorption of O radicals is favored, as shown by the low-energy values of −2.09 eV at the O/aGNR/Cu(111) interface and −2.11 eV at O/zGNR/Cu(111) interface. Our BE_{O_2} calculations indicate that the bridge-type three-fold hollow site adsorption configuration yields a higher energy gain per O atom (Figure 3a(iv),b(iii)) when compared to the molecular adsorption of O_2 on the Cu surface.

Of particular interest is the effect of oxygen confinement on the BE_{O_2} value, where O atoms are inserted and confined between the GNR and Cu, as depicted in Figures S2c−e and S3e(i). As the dissociated O_2 adsorbs closer to the GNR, the confinement effects become more significant and the oxygen adsorption energy is reduced. For the aGNR/Cu(111) system, the calculated BE_{O_2} value decreased from −3.46 to −2.95 eV/O_2, whereas for the zGNR/Cu(111) system, the calculated BE_{O_2} value decreased from −3.34 to −2.72 eV/O_2. We attribute the larger oxygen adsorption energy calculated for the aGNR/Cu(111) (Figure S2c) and zGNR/Cu(111) (Figure S3i) systems to the interaction between the CH groups in the nanoribbon and the adsorbed oxygen. Furthermore, our BE_{O_2} calculations also show that the presence of adsorbed oxygen species (dissociated and nondissociated) at the GNR/Cu(111) edge sites enhances the interaction between the GNR and the Cu(111) surface, compared to that for O atoms confined between the GNR and Cu away from the edges (Figures S2e and S3e). The binding energy between GNR and O/Cu(111) indicates that the GNR adsorption interaction at the edge site is enhanced for both the armchair and zigzag systems, as determined by the calculated BE_{GNR} values of −1.96 and −2.84 eV in Figures S2c and S3i, respectively. For the O atoms confined between the GNR and Cu, the GNR adsorption is relatively weakened (Figures S2e and S3e).

The bond length of an isolated O_2 molecule is calculated to be 1.23 Å, which is close to the experimental bond length of 1.21 Å.[53] When adsorbed molecularly at the GNR/Cu(111) interface, the O−O bond can be elongated to ∼1.46−1.53 Å. To our knowledge, the experimental intramolecular stretching mode for O_2 adsorbed at GNR/Cu at low temperatures has not been reported. We calculated the O_2 vibrational stretching frequency, ν(O−O), for the molecular O_2 adsorption at the bare Cu and GNR/Cu sites (see Supporting Information). The ν(O−O) for an isolated O_2 molecule is within agreement (0.3% difference) with the experimental[54] and theoretical[49] values. When the O_2 molecule is adsorbed at either Cu(111) or GNR/Cu(111), the ν(O−O) is red-shifted, from 1561 to 635−776 cm^{-1}, which is in accordance with the characteristic of an elongated O−O bond.[49,54] While the larger magnitude of the red shift is calculated for O_2/GNR/Cu, the O_2/Cu adsorption interaction showed a slightly smaller red shift in comparison to the ν(O−O) in O_2/GNR/Cu. This pattern confirms the role of GNR edges in weakening the already elongated O−O bond at the GNR/Cu interface. Only the PDOS of a molecularly adsorbed O_2 at the zGNR/Cu(111) interface was calculated (Figure S5) due to the shortest O−O bond length of 1.46 Å in comparison with other structures. This short bond length indicates a hybridization between the O $2p_z$ and the Cu $3d_{z^2}$ states, while the aforementioned hybridization between the C $2p_z$ and the Cu $3d_{z^2}$ orbitals remain observable at the zigzag edge. The dissociation of O_2 on the Cu surface is accompanied by molecular transformations involving the topmost Cu atoms, where the Cu−O bond lengths are calculated to be ∼1.82−1.92 Å. Experimentally, the reconstruction of the Cu(111) surface, as opposed to Cu(100) and Cu(110), has been more closely associated with the Cu_2O(111) structure, in terms of both the Cu coordination and the Cu−O bond length.[55] Adsorption of the O radical pairs at the bridge site (Figure 3a(iv)) is not possible on the relaxed surface unless the Cu atom situated

DOI: 10.1021/jacs.6b05333
J. Am. Chem. Soc. 2016, 138, 10986−10994

between the O atoms is lifted upward.[52] This configuration was favored based on studies by high-resolution electron energy loss spectroscopy[56] and scanning tunneling microscopy.[55] Thus, the atomic displacement of Cu at the surface level also means a more corrugated substrate at the aGNR/Cu interface.

H_2O Adsorption Mechanism. As shown in Figure 3c,d, H_2O has a higher activation barrier for dissociation at the aGNR/Cu (0.72 eV) than at the zGNR/Cu (0.43 eV) edge site, and notably, these values are higher than those measured for analogous processes that involve O_2. However, for the H_2O dissociation at bare Cu(111), previous theoretical studies have reported much higher activation barriers of 1.01−1.40 eV[20,57,58] and the experimentally determined value has been reported to be 1.17 eV.[59] Nevertheless, the slightly endothermic H_2O reaction at zGNR/Cu further indicated that the O_2 dissociation mechanism is thermodynamically more plausible, in which the GNRs play a non-negligible role in reducing the activation barriers for both O_2 and H_2O dissociations. The influence of H_2O in heterogeneous reactions is noticeably different from the mechanism by which H_2O is dissociated on clean Cu surfaces because both GNR and the preadsorbed oxygen atoms can act like reactants and influence the H_2O dissociation. For instance, the adsorption of H_2O on Cu is stabilized by the presence of the GNR functional groups, as indicated by the stronger BE value for both aGNR/Cu and zGNR/Cu systems (−0.47 and −0.45 eV), compared to the molecular adsorption of water on bare Cu (−0.26 and −0.23 eV). Previous experimental[60] and theoretical[20,61] studies have reported the BE value for H_2O adsorption on bare Cu(111) to be −0.40 eV and −0.16 to −0.22 eV, respectively. Instead of having the water O−H group facing either the vacuum or the Cu surface, the physisorption of H_2O on a bare Cu surface can be enhanced by the presence of (i) O atoms on Cu(111) and (ii) the GNR C−H groups. At the aGNR as well as the zGNR edges, the H_2O molecules were calculated to be stabilized by the adsorption interactions between the C−H groups in the GNRs and the O−H groups of H_2O, with $H_{GNR}-O_{H_2O}$ distances of 2.34−2.37 Å. Next, we calculate the H_2O adsorption energy in the presence of both preadsorbed O species and GNR on Cu(111) (see Tables S1 and S2 of SI). For the O/aGNR/Cu as well as the O/zGNR/Cu interfaces, the strongest configuration for H_2O adsorption can be described by the $H_{H_2O}-O_{ads}$ interactions, where water molecules interact with oxygen atoms present at the surface, while the O_{H_2O} atom interacts with the Cu surface. Such an orientation of H_2O appears to be significantly more stable than the other configuration, where the H_{H_2O} atoms are also O-radical-stabilized, but with the O_{H_2O} atom approaching the GNR functional group. Based on these findings, we propose that the graphene edge facilitates the stabilization of H_2O (regardless of the surface oxygenation), which would otherwise be unstable. H_2O showed a weaker binding energy in the absence of GNR and surface O radicals. In the following section, we describe H_2O intercalation using the preadsorbed and preintercalated O/GNR/Cu models.

Oxygen-Assisted H_2O Adsorption and Intercalation. Using the dissociated products shown in Figure 3a,b as a model, we calculated the H_2O adsorption interaction energy at the O+O/GNR/Cu(111) interface. Additionally, we also consider the possible reaction pathways for the zGNR/Cu decoupling as facilitated by the dissociative O_2 intercalation along with H_2O dissociation. This reaction mechanism is important when considering the relatively small activation barrier (0.32−0.37 eV) for atomic oxygen intercalation at the aGNR/Cu (Figure S6a) and zGNR/Cu (Figure 5) interfaces. Figures 4 and 5b show the energy profile along the H_2O dissociation path at the aGNR/Cu(111) and zGNR/Cu(111) interfaces, respectively. This observed modification of the

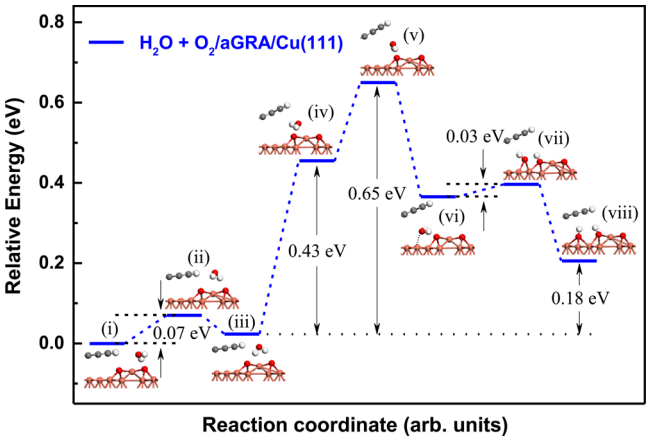

Figure 4. NEB calculation of the adsorption of O_2 + H_2O (blue) at the aGNR/Cu(111) interface, showing the reaction barrier for H_2O intercalation.

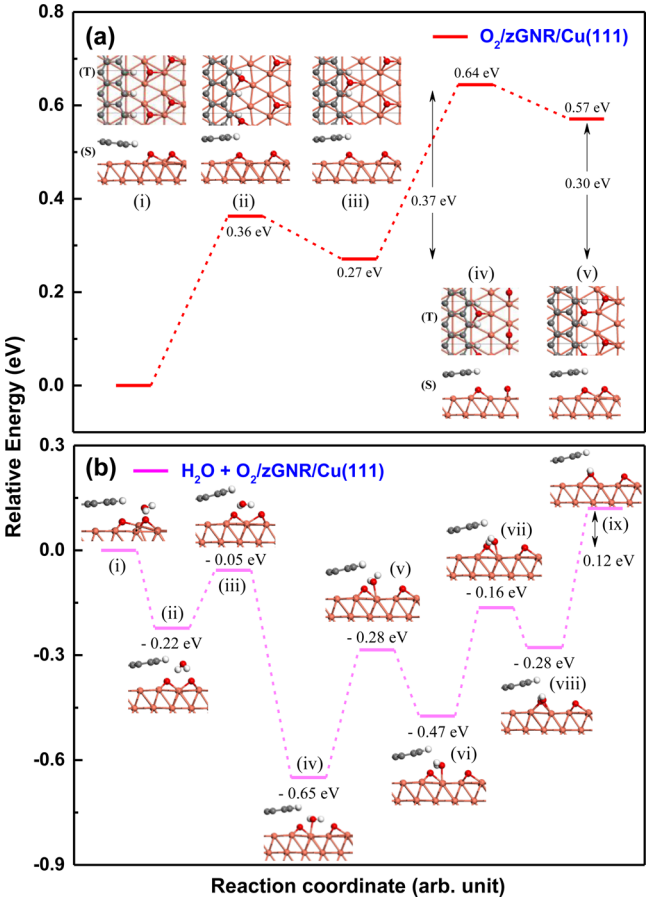

Figure 5. NEB calculations showing (a) top and side views of O_2 intercalation at the zGNR/Cu(111) interface, (b) adsorption of H_2O (pink) at the O-intercalated zGNR/Cu(111) interface, showing side views only.

DOI: 10.1021/jacs.6b05333
J. Am. Chem. Soc. 2016, 138, 10986−10994

GNR/Cu interface implies that GNR-mediated interactions between H_2O and the chemisorbed O radicals can be important in elucidating the role of H_2O and O_2 in the surface oxide formation. The activation barrier for O atom intercalation at the interface is ~0.33 eV (0.40 eV per molecule) for aGNR/Cu and ~0.37 eV (0.64 eV per molecule) for zGNR/Cu. The barrier for O_2 diffusion at H_2O-covered Cu(111) has been calculated experimentally (0.20 eV for bulk water[62]) and theoretically (0.32−0.36 eV for hexagonally ordered water layers on Cu(111)[63]). The small energy difference between the two chemical reactions (the O atom intercalation at GNR/Cu and O_2 diffusion in water) indicates that both reactions can occur concurrently. For the armchair system, the energy difference between the reactant and the product (ΔE) for the H_2O intercalation (0.65 eV) and dissociation (0.03 eV) at O +O/aGNR/Cu(111) reveals that this intercalation process may be slightly endothermic (energy increases by 0.18 eV), indicating an insufficiency of thermodynamics or kinetics to drive the chemical transformation of H_2O to OH groups at the O-doped sites at 0 K. However, previous XPS and AES studies have indicated that copper(II) hydroxide is always created during the electrochemical corrosion process in Cu, as a direct result of the reaction of copper and hydroxyl ions ($Cu^{2+} + 2OH^- \rightarrow Cu(OH)_2$).[64,65] Here the hydrogen bond interaction and the OH bond cleavage are seen along the reaction pathway. The presence of oxygen species (as well as GNR) promotes the H_2O dissociation remarkably. Nonetheless, this effect is also dependent on the location of H_2O as molecular dissociation occurs only under the GNR layer with a negligibly small activation barrier. Our calculated dissociation activation barrier of −0.26 eV for H_2O at the O/aGNR/Cu(111) site is smaller than the activation barrier previously reported for the dissociation of H_2O at Cu(111) (−1.01 eV)[57] and at O/Cu(111) (−0.36 eV),[63] indicating an effect that may originate from the surface oxygen and the GNR on H_2O dissociation. Our H_2O intercalation activation barrier at the aGNR/Cu site is lower than that reported for O atom diffusion (2.86 eV) at graphene/Cu(111) surface defects composed of heptagonal Stone−Wales defects with OH functional groups.[66] The relatively smaller activation barriers in our study implies that the O intercalation at graphene defect sites on Cu(111) could be energetically less favorable than the decoupling of aGNR on Cu(111).

For the zigzag system, H_2O is adsorbed at the O-preintercalated zGNR/Cu interface, as shown in Figure 5a(v). Unlike the armchair system, H_2O can be first stabilized by the $H_{H_2O}-O_{ads}$ interaction above the surface O radicals followed by the displacement of an O radical that leads to the exothermic adsorption on the Cu surface. The interaction between H_{H_2O} and O_{ads} is followed by H_2O bond cleavage that results in the formation of surface hydroxyls—the OH_{ads} formation is slightly endothermic. If the H_2O cleaving reaction proceeds beyond the state of surface hydroxyls, the dissociation of O−H groups could play a role in propagating the oxide layer formation. The detailed mechanism of H (or H_2) generation via the OH bond scission is not covered in the armchair and zigzag systems in our study. However, we note that hydrogen generation via the direct scission of the OH bond ($OH_{ads} \rightarrow O_{ads} + H_{ads}$) has a calculated activation barrier of 1.76 eV, while the formation of H_2O via two neighboring OH groups ($2OH_{ads} \rightarrow H_2O_{ads} + O_{ads}$) can have a smaller activation barrier to overcome (0.23 eV).[20] Such a small barrier could be an important factor in driving the intercalation of H_2O molecules further under nanoscopic confinements by the formation of hydrogen-bonded arrangements at the O-doped GNR/Cu interfaces. Overall, we demonstrate that the dissociation of O_2 is exothermic at both aGNR/Cu and zGNR/Cu. However, the dissociation of H_2O is less stable (endothermic) at the O/aGNR/Cu and O/zGNR/Cu interfaces with activation barriers of 0.03 and 0.31 eV, respectively. It is thus possible to identify the physicochemical properties of adsorbate molecule(s) at the GNR/Cu(111) interfaces depending on the graphene edge type.

The upward bending of the aGNR is illustrated in Figure S8 in terms of the edge Cu separation and the relative total energy of each structure. The optimized geometries for H_2O intercalation and dissociation at the aGNR/Cu interface appear to be less favorable when compared to the O_2 dissociation, due to the larger activation barrier and higher potential energy. However, water intercalation is still favorable at low temperatures, in view of the ~1.01−1.28 eV energy required for H_2O dissociation on the bare Cu surface. For the zigzag system, we demonstrate that H_2O intercalation can occur following O_2 intercalation at the interface. For the case of the O-doped zGNR/Cu, O_2 dissociation is located away from the zGNR edge, at a distance larger than that for the O-doped aGNR/Cu system. Thus, H_2O intercalation in the zGNR/Cu is impeded due to the subtle interplay of the zGNR/Cu hybridization and the proximity of the water molecule to the nearest O species adsorbed on the substrate. This is demonstrated by the fact that both interlayer distances and the zGNR binding energy remain unchanged upon H_2O dissociation on the surface. Hence, we suggest that zGNR can offer better protection against oxidation in copper when compared to an aGNR.

CONCLUSIONS

In summary, a first-principles study of the adsorption interactions of O_2 and H_2O at the GNR/Cu interface, leading to adsorbate-induced decoupling of GNR/Cu, has been presented. The presence of the GNR edge can significantly reduce the activation barrier for the dissociation of O_2 and H_2O on Cu(111), indicating a stronger oxide-forming tendency when compared to the bare Cu surface. The calculated red shift in the O−O vibrational stretching mode for O_2/GNR/Cu distinguished the role of GNR in the molecular adsorptions of O_2. The overall dissociative adsorption of O_2 at the GNR/Cu edges is exothermic with very small E_a values of 0.025 and 0.032 eV for the aGNR/Cu and zGNR/Cu edges, respectively. The configuration of O atoms at the GNR/Cu interface can lead to the following: (i) surface reconstruction of Cu(111), (ii) enhanced adsorption interaction between GNR and the Cu substrate due to the stabilization of the edge C−H functional group, and (iii) weakened adsorption interaction between GNR and the Cu substrate due to the intercalation of oxygen. H_2O has a limited range of adsorption configurations on bare Cu(111) but can be stabilized by additional interactions in the presence of GNRs. We show that the dissociation of H_2O is directly involved in the formation of hydroxyl groups ($H_2O + O_{ads} \rightarrow OH_{ads} + OH_{ads}$); H_2O preferentially dissociates when confined at the aGNR/Cu interface but does not dissociate readily outside the GNR unless O-doped surface is present. The dissociation of H_2O at the oxygen preadsorbed GNR/Cu interface is thermodynamically favored with a relatively small energy difference between the reactant and the product (ΔE of 0.12−0.18 eV). Therefore, we deduce that, during the initial

DOI: 10.1021/jacs.6b05333
J. Am. Chem. Soc. 2016, 138, 10986−10994

stages of the Cu(111) oxidation process at the graphene edge sites, oxygen can originate from both O_2 and H_2O.

The intrinsic π−d hybridization between zGNR and Cu observed in this study is attributed to the covalent-like bonding interaction at the edge site, which in turn leads to the strong adhesion of the zGNR edge to the Cu substrate. Based on NEB simulations for molecular dissociation and intercalation at the GNR/Cu interfaces, however, we have identified the possible mechanisms for GNR/Cu decoupling. As a first step, a dissociative chemisorption of O_2, followed by H_2O dissociation, provides a low activation barrier route for GNR/Cu decoupling. Alternatively, intercalation of O_2 can also facilitate the subsequent H_2O intercalation at the zGNR/Cu interface, even though this process is thermodynamically less favorable than having O_2 dissociation as the first step toward GNR/Cu decoupling. The results obtained in this work clearly illustrate the influence of the edge terminations of submonolayer graphene islands on the oxidation or hydroxylation of the underlying metal surface, thereby controlling the structure and chemistry of graphene/Cu interfaces. The synergistic interaction between O_2 and the dissociative adsorption interaction of H_2O at the GNR/Cu edge sites may have interesting implications for the development of regioselective graphene-based catalysis.

■ ASSOCIATED CONTENT

Supporting Information

The Supporting Information is available free of charge on the ACS Publications website at DOI: 10.1021/jacs.6b05333.

Binding energies and structural properties of O_2 and H_2O adsorbed at GNR/Cu(111) interfaces; PDOS of H atoms at GNR edges; PDOS of O_2/zGNR/Cu(111); reaction pathways for H_2O dissociation at both GNR/Cu(111) interfaces; intramolecular O−O stretching mode for adsorbed O_2; coordinates of the optimized geometries, including their absolute energies (in hartrees) (PDF)

■ AUTHOR INFORMATION

Corresponding Authors

*ruoff@unist.ac.kr

*skkwak@unist.ac.kr

Notes

The authors declare no competing financial interest.

■ ACKNOWLEDGMENTS

This work was supported by IBS-R019-D1 and NRF-2014R1A5A1009799. Computational resources were used from CMCM, UNIST-HPC, and KISTI (KSC-2016-C2-0003). The authors thank Revathi R. Bacsa for useful discussions and critical reading of the manuscript. The authors thank Xueqiu You and Da Luo for fruitful discussions.

■ REFERENCES

(1) Li, X.; Cai, W.; An, J.; Kim, S.; Nah, J.; Yang, D.; Piner, R.; Velamakanni, A.; Jung, I.; Tutuc, E.; Banerjee, S. K.; Colombo, L.; Ruoff, R. S. *Science* **2009**, *324*, 1312−1314.

(2) Lu, A.-Y.; Wei, S.-Y.; Wu, C.-Y.; Hernandez, Y.; Chen, T.-Y.; Liu, T.-H.; Pao, C.-W.; Chen, F.-R.; Li, L.-J.; Juang, Z.-Y. *RSC Adv.* **2012**, *2*, 3008−3013.

(3) Gupta, P.; Dongare, P. D.; Grover, S.; Dubey, S.; Mamgain, H.; Bhattacharya, A.; Deshmukh, M. M. *Sci. Rep.* **2014**, *4*, 3882.

(4) Ogawa, S.; Yamada, T.; Ishidzuka, S.; Yoshigoe, A.; Hasegawa, M.; Teraoka, Y.; Takakuwa, Y. *Jpn. J. Appl. Phys.* **2013**, *52*, 110122.

(5) Sun, W.; Wang, L.; Wu, T.; Wang, M.; Yang, Z.; Pan, Y.; Liu, G. *Chem. Mater.* **2015**, *27*, 2367−2373.

(6) Schriver, M.; Regan, W.; Gannett, W. J.; Zaniewski, A. M.; Crommie, M. F.; Zettl, A. *ACS Nano* **2013**, *7*, 5763−5768.

(7) Nam, T.-H.; Lee, J.-H.; Choi, S.-R.; Yoo, J.-B.; Kim, J.-G. *Int. J. Hydrogen Energy* **2014**, *39*, 11810−11817.

(8) Blume, R.; Kidambi, P. R.; Bayer, B. C.; Weatherup, R. S.; Wang, Z.-J.; Weinberg, G.; Willinger, M.-G.; Greiner, M.; Hofmann, S.; Knop-Gericke, A.; Schlogl, R. *Phys. Chem. Chem. Phys.* **2014**, *16*, 25989−26003.

(9) Zhang, W.-B.; Chen, C. *J. Phys. D: Appl. Phys.* **2015**, *48*, 015308.

(10) Sutter, P.; Sadowski, J. T.; Sutter, E. A. *J. Am. Chem. Soc.* **2010**, *132*, 8175−8179.

(11) Grånäs, E.; Andersen, M.; Arman, M. A.; Gerber, T.; Hammer, B.; Schnadt, J.; Andersen, J. N.; Michely, T.; Knudsen, J. *J. Phys. Chem. C* **2013**, *117*, 16438−16447.

(12) Nilsson, L.; Andersen, M.; Balog, R.; Lægsgaard, E.; Hofmann, P.; Besenbacher, F.; Hammer, B.; Stensgaard, I.; Hornekær, L. *ACS Nano* **2012**, *6*, 10258−10266.

(13) Jin, L.; Fu, Q.; Dong, A.; Ning, Y.; Wang, Z.; Bluhm, H.; Bao, X. *J. Phys. Chem. C* **2014**, *118*, 12391−12398.

(14) Feng, X.; Maier, S.; Salmeron, M. *J. Am. Chem. Soc.* **2012**, *134*, 5662−5668.

(15) Kidambi, P. R.; Bayer, B. C.; Blume, R.; Wang, Z.-J.; Baehtz, C.; Weatherup, R. S.; Willinger, M.-G.; Schloegl, R.; Hofmann, S. *Nano Lett.* **2013**, *13*, 4769−4778.

(16) Gattinoni, C.; Michaelides, A. *Surf. Sci. Rep.* **2015**, *70*, 424−447.

(17) Wu, R.; Gan, L.; Ou, X.; Zhang, Q.; Luo, Z. *Carbon* **2016**, *98*, 138−143.

(18) Johnston, S. M.; Mulligan, A.; Dhanak, V.; Kadodwala, M. *Surf. Sci.* **2002**, *519*, 57−63.

(19) Ford, D. C.; Nilekar, A. U.; Xu, Y.; Mavrikakis, M. *Surf. Sci.* **2010**, *604*, 1565−1575.

(20) Wang, G.-C.; Nakamura, J. *J. Phys. Chem. Lett.* **2010**, *1*, 3053−3057.

(21) Zhou, S.; Bongiorno, A. *Sci. Rep.* **2013**, *3*, 2484.

(22) Bagri, A.; Mattevi, C.; Acik, M.; Chabal, Y. J.; Chhowalla, M.; Shenoy, V. B. *Nat. Chem.* **2010**, *2*, 581−587.

(23) Ago, H.; Ohta, Y.; Hibino, H.; Yoshimura, D.; Takizawa, R.; Uchida, Y.; Tsuji, M.; Okajima, T.; Mitani, H.; Mizuno, S. *Chem. Mater.* **2015**, *27*, 5377−5385.

(24) Brown, L.; Lochocki, E. B.; Avila, J.; Kim, C.-J.; Ogawa, Y.; Havener, R. W.; Kim, D.-K.; Monkman, E. J.; Shai, D. E.; Wei, H. I.; Levendorf, M. P.; Asensio, M.; Shen, K. M.; Park, J. *Nano Lett.* **2014**, *14*, 5706−5711.

(25) Nguyen, V. L.; Shin, B. G.; Duong, D. L.; Kim, S. T.; Perello, D.; Lim, Y. J.; Yuan, Q. H.; Ding, F.; Jeong, H. Y.; Shin, H. S.; Lee, S. M.; Chae, S. H.; Vu, Q. A.; Lee, S. H.; Lee, Y. H. *Adv. Mater.* **2015**, *27*, 1376−1382.

(26) Chen, X.; Zhao, P.; Xiang, R.; Kim, S.; Cha, J.; Chiashi, S.; Maruyama, S. *Carbon* **2015**, *94*, 810−815.

(27) Wassmann, T.; Seitsonen, A. P.; Saitta, A. M.; Lazzeri, M.; Mauri, F. *Phys. Rev. Lett.* **2008**, *101*, 096402.

(28) Girit, Ç. Ö.; Meyer, J. C.; Erni, R.; Rossell, M. D.; Kisielowski, C.; Yang, L.; Park, C.-H.; Crommie, M. F.; Cohen, M. L.; Louie, S. G.; Zettl, A. *Science* **2009**, *323*, 1705−1708.

(29) Zhang, X.; Wang, L.; Xin, J.; Yakobson, B. I.; Ding, F. *J. Am. Chem. Soc.* **2014**, *136*, 3040−3047.

(30) Kresse, G.; Furthmuller, J. *Phys. Rev. B: Condens. Matter Mater. Phys.* **1996**, *54*, 11169−11186.

(31) Kresse, G.; Furthmüller, J. *Comput. Mater. Sci.* **1996**, *6*, 15−50.

(32) Kresse, G.; Joubert, D. *Phys. Rev. B: Condens. Matter Mater. Phys.* **1999**, *59*, 1758−1775.

(33) Perdew, J. P.; Burke, K.; Ernzerhof, M. *Phys. Rev. Lett.* **1996**, *77*, 3865.

(34) Grimme, S. *J. Comput. Chem.* **2006**, *27*, 1787−1799.

DOI: 10.1021/jacs.6b05333
J. Am. Chem. Soc. 2016, 138, 10986−10994

(35) Henkelman, G.; Uberuaga, B. P.; Jónsson, H. *J. Chem. Phys.* **2000**, *113*, 9901−9904.
(36) Henkelman, G.; Jónsson, H. *J. Chem. Phys.* **2000**, *113*, 9978−9985.
(37) Kawai, T.; Miyamoto, Y.; Sugino, O.; Koga, Y. *Phys. Rev. B: Condens. Matter Mater. Phys.* **2000**, *62*, R16349−R16352.
(38) Ma, L.; Zeng, X. C.; Wang, J. *J. Phys. Chem. Lett.* **2015**, *6*, 4099−4105.
(39) Li, X.; Feng, J.; Wang, E.; Meng, S.; Klimeš, J.; Michaelides, A. *Phys. Rev. B: Condens. Matter Mater. Phys.* **2012**, *85*, 085425.
(40) Artyukhov, V. I.; Hao, Y.; Ruoff, R. S.; Yakobson, B. I. *Phys. Rev. Lett.* **2015**, *114*, 115502.
(41) Wang, Q.; Wei, L.; Sullivan, M.; Yang, S.-W.; Chen, Y. *RSC Adv.* **2013**, *3*, 3046−3053.
(42) Giovannetti, G.; Khomyakov, P. A.; Brocks, G.; Karpan, V. M.; van den Brink, J.; Kelly, P. J. *Phys. Rev. Lett.* **2008**, *101*, 026803.
(43) Khomyakov, P. A.; Giovannetti, G.; Rusu, P. C.; Brocks, G.; van den Brink, J.; Kelly, P. J. *Phys. Rev. B: Condens. Matter Mater. Phys.* **2009**, *79*, 195425.
(44) Mi, X.; Meunier, V.; Koratkar, N.; Shi, Y. *Phys. Rev. B: Condens. Matter Mater. Phys.* **2012**, *85*, 155436.
(45) Li, Y.; Zhang, W.; Morgenstern, M.; Mazzarello, R. *Phys. Rev. Lett.* **2013**, *110*, 216804.
(46) Li, Y.; Subramaniam, D.; Atodiresei, N.; Lazić, P.; Caciuc, V.; Pauly, C.; Georgi, A.; Busse, C.; Liebmann, M.; Blügel, S.; Pratzer, M.; Morgenstern, M.; Mazzarello, R. *Adv. Mater.* **2013**, *25*, 1967−1972.
(47) Jiang, D.-E.; Sumpter, B. G.; Dai, S. *J. Chem. Phys.* **2007**, *126*, 134701.
(48) Golubeva, E. N.; Zubanova, E. M.; Zhidomirov, G. M. *J. Phys. Org. Chem.* **2013**, *26*, 724−729.
(49) López-Moreno, S.; Romero, A. H. *J. Chem. Phys.* **2015**, *142*, 154702.
(50) Habraken, F. H. P. M.; Kieffer, E. P.; Bootsma, G. A. *Surf. Sci.* **1979**, *83*, 45−59.
(51) Fujita, K.; Ando, D.; Uchikoshi, M.; Mimura, K.; Isshiki, M. *Appl. Surf. Sci.* **2013**, *276*, 347−358.
(52) Xu, Y.; Mavrikakis, M. *Surf. Sci.* **2001**, *494*, 131−144.
(53) Kerr, J. A. *Anal. Chim. Acta* **1982**, *144*, 298.
(54) Sueyoshi, T.; Sasaki, T.; Iwasawa, Y. *Surf. Sci.* **1996**, *365*, 310−318.
(55) Jensen, F.; Besenbacher, F.; Lægsgaard, E.; Stensgaard, I. *Surf. Sci.* **1991**, *259*, L774−L780.
(56) Dubois, L. H. *Surf. Sci.* **1982**, *119*, 399−410.
(57) Phatak, A. A.; Delgass, W. N.; Ribeiro, F. H.; Schneider, W. F. *J. Phys. Chem. C* **2009**, *113*, 7269−7276.
(58) Gokhale, A. A.; Dumesic, J. A.; Mavrikakis, M. *J. Am. Chem. Soc.* **2008**, *130*, 1402−1414.
(59) Campbell, C. T.; Daube, K. A. *J. Catal.* **1987**, *104*, 109−119.
(60) Thiel, P. A.; Madey, T. E. *Surf. Sci. Rep.* **1987**, *7*, 211−385.
(61) Fajín, J. L. C.; Illas, F.; Gomes, J. R. B. *J. Chem. Phys.* **2009**, *130*, 224702.
(62) Wong, C. F.; Hayduk, W. *Can. J. Chem. Eng.* **1990**, *68*, 849−859.
(63) Sumer, A.; Chaudhuri, S. *J. Chem. Phys.* **2015**, *142*, 124703.
(64) Wlasny, I.; Dabrowski, P.; Rogala, M.; Pasternak, I.; Strupinski, W.; Baranowski, J. M.; Klusek, Z. *Corros. Sci.* **2015**, *92*, 69−75.
(65) Platzman, I.; Brener, R.; Haick, H.; Tannenbaum, R. *J. Phys. Chem. C* **2008**, *112*, 1101−1108.
(66) Duong, D. L.; Han, G. H.; Lee, S. M.; Gunes, F.; Kim, E. S.; Kim, S. T.; Kim, H.; Ta, Q. H.; So, K. P.; Yoon, S. J.; Chae, S. J.; Jo, Y. W.; Park, M. H.; Chae, S. H.; Lim, S. C.; Choi, J. Y.; Lee, Y. H. *Nature* **2012**, *490*, 235−239.

DOI: 10.1021/jacs.6b05333
J. Am. Chem. Soc. 2016, 138, 10986−10994